Vacuum Ultraviolet Photoionization Mass Spectrometric Study of Ethylenediamine

ARTICLE *in* THE JOURNAL OF PHYSICAL CHEMISTRY A · AUGUST 2006

Impact Factor: 2.69 · DOI: 10.1021/jp061876g · Source: PubMed

Vacuum Ultraviolet Photoionization Mass Spectrometric Study of Ethylenediamine

Lixia Wei, Bin Yang, Jing Wang, Chaoqun Huang, Liusi Sheng, Yunwu Zhang, and Fei Qi*

National Synchrotron Radiation Laboratory, University of Science and Technology of China, Hefei, Anhui 230029, P. R. China

Chow-Shing Lam and Wai-Kee Li*

Department of Chemistry, The Chinese University of Hong Kong, Shatin, N.T., Hong Kong

Received: March 27, 2006; In Final Form: May 19, 2006

The photoionization and dissociative photoionizations of ethylenediamine have been studied both experimentally and theoretically. In experiments, photoionization efficiency spectra for ions $NH_2CHCH_3^+$, $NH_2CH{=}CH_2^+$, $CH_2NH_2^+$, NH_3^+, $NH_2CH_2CHNH_2^+$ and $NH_2CH_2CH_2NH_2^+$ have been obtained. In addition, the energetics of the dissociative photoionization is investigated with ab initio Gaussian-3 (G3) calculations. The computational results are useful in analyzing the dissociation channels near the ionization thresholds. With the help of the G3 results, the dissociation channels for the formation of the aforementioned fragment ions have been established.

Introduction

Ethylenediamine (en) is an important chemical industrial material. It is used extensively in the production of organic compounds, medicines, polymers, fuels, pesticides, and so on. In addition, it is also used in the production of chelators, anticorrosive compounds and lubricants. Indeed, en itself is an important chelating and analytical reagent. The chelated complexes of en are extensively used in many areas. Thus it is helpful to study the photoionization of en to understand the properties of this compound and its derivatives.

The ionization energy (IE) of en and the appearance energies (AEs) of its fragments have been reported previously.[1,2] Kimura et al. obtained the IE of en with HeI photoelectron spectroscopy.[1] Furthermore, Burkey et al. obtained the AE of the fragment ion $m/e = 30$ ($CH_2NH_2^+$) by the method of electron impact ionization.[2] Computationally, Radom et al. used ab initio molecular orbital theory to study the internal rotation in en.[3] Their conformational predictions are in agreement with the available experimental data. They also found that the factors influencing the conformational preferences include steric, dipolar, and hyperconjugative interactions and intramolecular hydrogen bonding. Alsenoy et al. determined 10 conformations of en by ab initio gradient geometry optimization with the 4-21G basis set.[4] Their calculations show that many energetically different conformers exist for the gauche and trans forms (with different N−C−C−N torsions) of the system. Kazerouni et al. analyzed the vapor-phase structures of the rotamers of en and the composition of the gaseous system at 343, 463, and 713 K from electron-diffraction data.[5] Lee et al. studied extensively the structures and conformational energies of en with ab initio molecular orbital theory.[6] They found that the major factor determining the conformational stabilities of the multiminima of en is the stereoelectronic effect and concluded that partial hydrogen bonding contributes to the structural stability of the two most stable structures of the isoenergetic gauche conformers. Chang et al. calculated the global conformational potentials of en at the MP2/6-311+G(2d,p) level by scanning through the dihedral angles of the two functional groups and the C−C bond with the remaining nuclear coordinates being energy-minimized.[7] With the global conformation potentials, they calculated the thermodynamic functions of the molecule and its individual conformers and also compared them with the gas-phase experimental thermodynamic data in the literature. Kudoh et al. measured the infrared spectra of en and its two deuterated species, $ND_2CH_2CH_2ND_2$ and $NH_2CD_2CD_2NH_2$, by matrix-isolation FTIR spectroscopy.[8] They found that isomerization around the central C−C axis from two gauche conformers to one trans conformer occurs upon infrared irradiation. They also made vibrational assignments with the aid of DFT calculations at the B3LYP level. Carvalho et al. performed a conformational analysis of en by both Raman spectroscopy and ab initio SCF-MO methods (with and without the inclusion of water solvent effects).[9] They investigated 10 different conformers by ab initio calculations and concluded from the Raman spectra that the conformational preferences are determined by the relative importance of intra- versus intermolecular hydrogen bonds. Besides, there are also many reports on the metal complexes of en, such as those of Ni,[10] Cu,[11] and Al, Ga, In, etc.[12] Nikos et al. investigated the complexation of Ni(II) by en in water/methanol solution with electrospray ionization mass spectrometry.[10] Wang et al. studied the Cu complex of en with the method of pulsed-filed ionization zero-electron kinetic energy (PFI-ZEKE) and ab initio calculations.[11] They measured the adiabatic IE and vibrational frequencies of the Cu-en stretch, Cu-en bend and hydrogen-bond stretch from the PFI-ZEKE spectrum.[11] They calculated the dissociation energies of these complexes as well. Yet so far there have been no reports on the photoionization of en. Efforts on the experiments of photoionization of en and the corresponding ab initio calculations are rather scarce.

In the present work, we report the photoionization efficiency (PIE) spectra of some fragment ions resulting from the dissociative photoionization of en in the photon energy region of 8−20 eV. From these PIE data, we can derive the energetics of

* Corresponding authors. F.Q.: e-mail, fqi@ustc.edu.cn; fax, +86-551-5141078. W.K.L.: e-mail, wkli@cuhk.edu.hk; fax, +852-26035057.

10.1021/jp061876g CCC: $33.50
Published on Web 06/24/2006

the dissociations. Combining these data with high level ab initio calculation results, the various dissociation channels of en can be established.

Experimental and Theoretical Methods

The experimental and computational methods employed in this work have been used to study, among others, the dissociations of ethylene oxide[13] and acetone.[14] A brief account of these methods is given below.

Experimental Method. The experimental setup has been described elsewhere,[13,15−17] and it will be concisely outlined here. Synchrotron radiation from the 800 MeV electron storage ring (National Synchrotron Radiation Laboratory, Hefei, China) is monochromatized by a 1 m Seya-Namioka monochromator equipped with two gratings (2400 and 1200 lines/mm) covering the wavelength range of 40−200 nm. The absolute wavelength of the monochromator was calibrated with the known IEs of inert gases. The wavelength resolution is about 0.2 nm at the wavelength of 100 nm with 150 μm entrance and exit slits. The photon flux was monitored by a silicon photodiode (SXUV-100, International Radiation Detectors, Inc.). A LiF window (1.0 mm thickness) was used to eliminate higher order radiation of the monochromized light in the wavelength region longer than 105 nm.

A reflectron time-of-flight (RTOF) mass spectrometry was employed for the VUV photoionization/fragmentation studies.[18] Photoions produced by the VUV light were drawn out of the photoionization region by a pulse extraction field triggered with a pulse generator (DG 535, SRS) and detected by a microchannel plate (MCP) detector. A voltage of 160 V was used to extract the ions into TOFMS. The ion signal was recorded by a multichannel scaler P7888 (FAST Comtec, Germany) after it was amplified with a preamplifier VT120C (EG & G, ORTEC). The total length of the ion flight is 1400 mm. The PIE spectra can be obtained as the wavelength scans with the increment of 0.2 nm.

The vapor of en (purity 99%) was introduced by supersonic expansion through a continuous beam nozzle (75 μm diameter) from the molecular beam chamber into the ionization chamber through a 1.0 mm skimmer. In this experiment, He (purity 99.99%) was used as the carrier gas and the stagnation pressure was about 0.1 MPa. The pressure of the ionization chamber was about 3.0×10^{-4} Pa when the molecule beam was introduced. No cluster was observed under this condition, so no fragment ions were considered to originate from cluster dissociation. With the same setup, the ionization energies of some stable molecules, such as N_2, O_2, CO_2, H_2O, etc. are measured. The results are in good agreement with the values in the literature. The extraction voltage of 160 V is not enough to cause the field ionization.

Computational Method. The ab initio model adopted in this work was the Gaussian-3 (G3) method, which is an approximation for the QCISD(T)/G3 large energy. It involves single-point calculations at the MP4/6-31G(d), MP4/6-31+G(d), MP4/6-31G(2df,p) and MP2(Full)/G3 large levels, all carried out with the structures optimized at the MP2(Full)/6-31+G(d) level. The MP2(Full)/6-31+G(d) harmonic frequencies, scaled by 0.9700, are used for the correction of zero-point vibrational energies (ZPVEs). A small semiempirical correction is also applied to account for the high level correlation effect. We have applied this method to a variety of chemical systems.[13,14] The agreement between G3 and experimental results is usually well within 0.15 eV for species with a few (less than 10) non-hydrogen atoms.

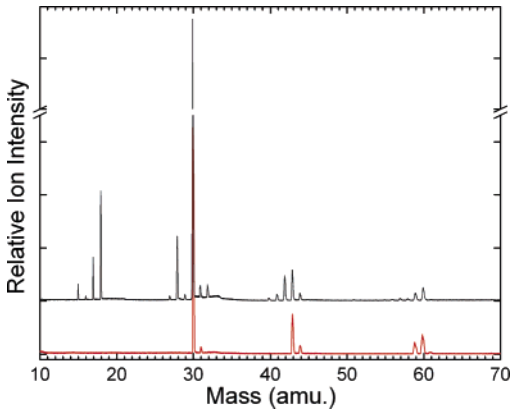

Figure 1. Photoionization mass spectrum of en at the wavelength of 55.0 nm (22.54 eV, upper curve) and 110.0 nm (11.27 eV, lower curve).

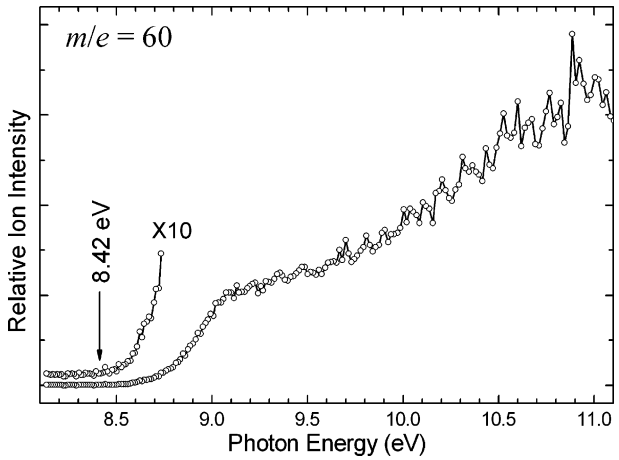

Figure 2. Photoionization efficiency curve of mass 60 ($C_2H_8N_2^+$) from photoionization of en.

All the computations involved in this work were carried out on various workstations and PCs using the Gaussian03 suite of programs.[19]

Results and Discussion

Experimental Measurements. The photoionization mass spectrum of en at the wavelength of 55.0 nm is shown in Figure 1, together with that taken at 110.0 nm. The latter was obtained with a LiF window to eliminate high-order radiation. As can be seen from the figure, in addition to the parent ion $C_2H_8N_2^+$ and the major fragment ions CH_4N^+ and $C_2H_5N^+$, other smaller fragment ions can also be identified. The mass peaks at $m/e =$ 18, 28 and 32 in the high-energy region can be ignored because they originate from the photoionization of background water and air.

The PIE spectra of the parent ion $C_2H_8N_2^+$ and of the fragment ions CH_4N^+, CH_3^+, NH_3^+, $C_2H_3^+$, $C_2H_4^+$, $C_2H_4N^+$, $C_2H_5N^+$, $C_2H_6N^+$, $C_2H_4N_2^+$, $C_2H_5N_2^+$, $C_2H_6N_2^+$ and $C_2H_7N_2^+$ from en were obtained by scanning photon energy. The PIE spectra of the parent ion $C_2H_8N_2^+$ ($m/e = 60$) and the fragment ion CH_4N^+ ($m/e = 30$) are shown in Figures 2 and 3, respectively, whereas those of $C_2H_5N^+$ ($m/e = 43$), $C_2H_6N^+$ ($m/e = 44$) and $C_2H_7N_2^+$ ($m/e = 59$) are displayed in Figure 4. The AE of each fragment was determined by the onset in each PIE spectrum. It should be pointed out that we ignored the thermal energy distribution of the parent molecule in our data treatment, considering the nozzle expansion condition described above. In addition, no correction was made for possible kinetic shifts in determining the AEs.

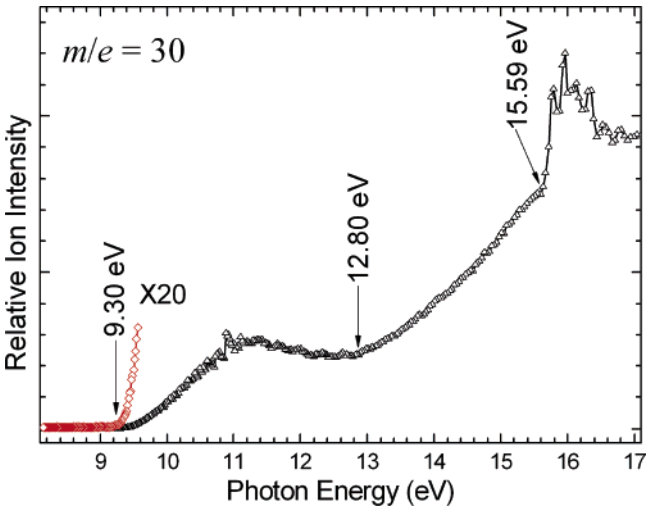

Figure 3. Photoionization efficiency curve of mass 30 (CH_4N^+) from dissociative photoionization of en.

All the AEs obtained from the PIE spectra are listed in Table 1, along with the values measured previously by other researchers. The error ranges are also listed. These errors reflect either the bandwidth of our monochromator or ionization threshold uncertainty on the PIE spectra. It should be pointed out that, in measuring the AEs of CH_4N^+, CH_5N^+, $C_2H_5N^+$, $C_2H_6N^+$, $C_2H_7N_2^+$ and $C_2H_8N_2^+$ in the low energy range, a LiF filter was used to eliminate the effect of higher-order radiation from the grating.

Computational Results. The structural formulas of the polyatomic species (with more than three atoms) involved in this work, along with their symmetry point groups and electronic states, are displayed in Figure 5. The calculated G3 energies of various species involved in the dissociations of en and its cation are summarized in Table 2. With the aid of these results, we will attempt to establish a number of dissociation channels for the en cation en^+.

To calculate the IE of en, it is necessary to determine the most stable conformation of en, because different conformers lead to different IEs. At the MP2(Full)/6-31+G(d) level, three representative conformers, namely **1**, **1′** and **1″**, have been identified. Their symmetry point groups are C_1, C_2 and C_{2h}, respectively. Conformer **1**, with an intramolecular hydrogen bond formed between the two amino groups, is the most stable among the three. The G3 energies of **1′** and **1″** relative to **1** are 2.3 and 5.2 kJ mol^{-1}, respectively. On the basis of the symmetry of these conformers, we have also derived three conformers for en^+, namely, **2**, **2′** and **2″**, which retain the symmetry of the neutrals **1**, **1′** and **1″**, respectively. With the E_0(G3) values of the various conformers of en and en^+, the IEs of **1**, **1′** and **1″** are calculated to be 8.54, 8.44 and 8.25 eV, respectively. Although the IE of **1′** appears to be in best agreement with the experimental result, 8.42 ± 0.04 eV, and the IE of **1″** is the lowest, they are not taken as the theoretical value. This is because there is significant geometric change for the ionization processes of **1′** → **2′** and **1″** → **2″**. On the other hand, conformer **1** has the most stable conformation and ionization **1** → **2** involves only minor structural change. Therefore, **1** → **2** is considered as the primary ionization process and the G3 IE of 8.54 eV is still in fairly good agreement with the experiment value. From here on, ion **2** is taken as the parent ion in the establishment of various dissociation channels to be discussed below.

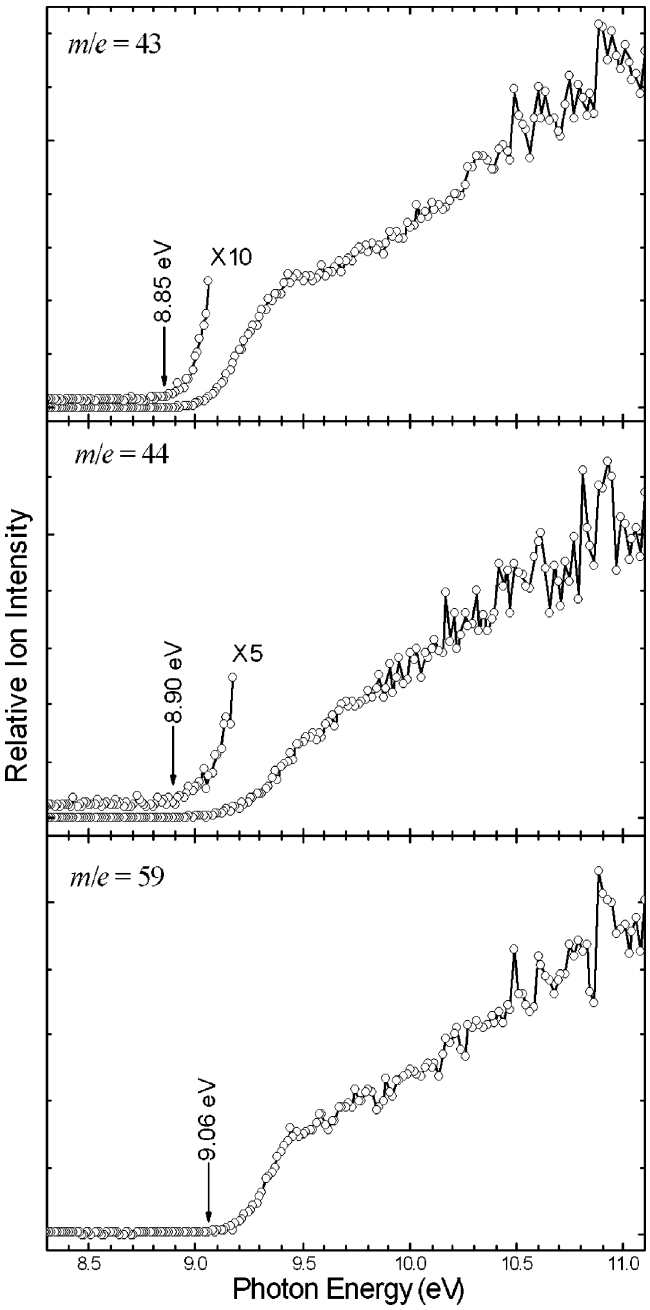

Figure 4. Photoionization efficiency curves of mass 43 ($C_2H_5N^+$), 44 ($C_2H_6N^+$) and 59 ($C_2H_7N_2^+$) from dissociative photoionization of en.

TABLE 1: Appearance Energies (eV) Measured in the Dissociative Photoionizations of En

m/e	ion	this work	previous
17	NH_3^+	14.54 ± 0.04	
30	$CH_2NH_2^+$	9.30 ± 0.03	9.56[2]
	$CH_2NH_2^+$	12.80 ± 0.06	
	$CH_2NH_2^+$	15.59 ± 0.06	
43	$C_2H_5N^+$	8.85 ± 0.03	
44	$C_2H_6N^+$	8.90 ± 0.03	
59	$C_2H_7N_2^+$	9.06 ± 0.03	
60	$NH_2CH_2CH_2NH_2^+$	8.42 ± 0.04	8.6[1]

Dissociation Channels of Cation En^+. When undergoing ionization, compounds with amino group(s) will lose one of the lone pair electrons on one of the nitrogen atom(s). This is certainly true for en. After being formed, en^+ will then undergo a series of dissociation to produce various fragment ions. Dissociations of the en^+ cation, which involve either only the

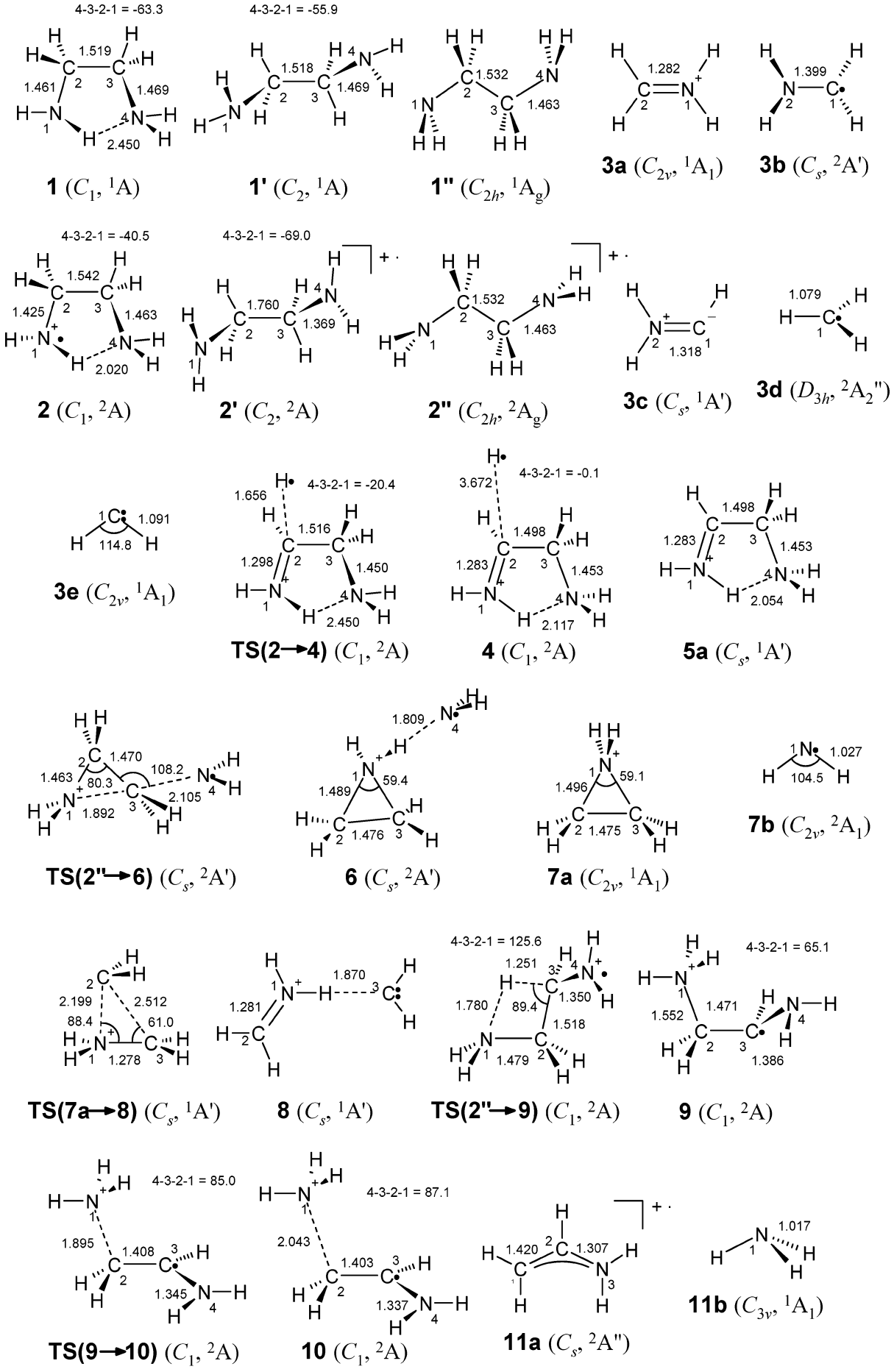

Figure 5. Cont'd.

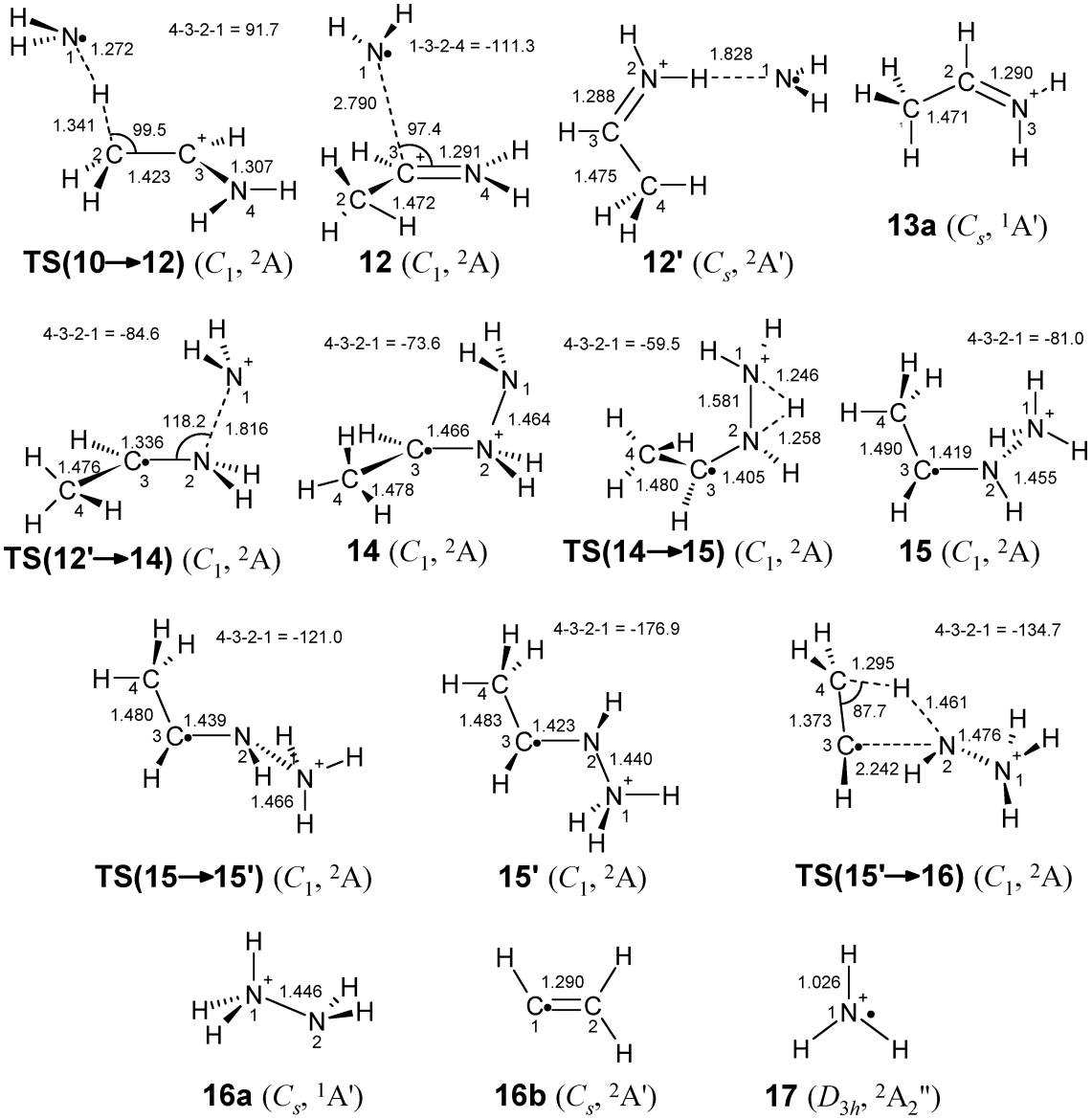

Figure 5. Structural formulas of the various polyatomic species (with more than three atoms) involved in this work, along with their symmetry point groups and electronic states.

TABLE 2: G3 Energies E_0 and H_{298} of Various Species Involved in the Dissociation of En and Its Cation

	E_0 (hatrees)	H_{298} (hatrees)		E_0 (hatrees)	H_{298} (hatrees)
1	−190.34234	−190.33609	**TS(15→15′)**	−189.98719	−189.98093
1′	−190.34154	−190.33523	**15′**	−189.98979	−189.98283
1″	−190.34060	−190.33411	**TS(15′→16)**	−189.86520	−189.85816
2	−190.02841	−190.02229	**3a**	−94.88275	−94.87881
2′	−190.03132	−190.02467	**3b**	−95.11140	−95.10708
2″	−190.03741	−190.03064	**3c**	−94.49672	−94.49280
TS(2→4)	−189.99205	−189.98590	**3d**	−39.79126	−39.78722
4	−190.00202	−189.99374	**3e**	−39.11053	−39.10674
TS(2″→6)	−189.97209	−189.96498	**5a**	−189.49901	−189.49323
6	−190.00811	−190.00064	**5b**	−0.50100	−0.50100
TS(2″→9)	−190.00571	−189.99951	**7a**	−134.14244	−134.13819
9	−190.05126	−190.04472	**7b**	−55.83753	−55.83375
TS(9→10)	−190.04989	−190.04317	**TS(7a→8)**	−133.99415	−133.98863
10	−190.05017	−190.04275	**8**	−134.01410	−134.00724
TS(10→12)	−190.00911	−190.00190	**11a**	−133.52771	−133.52296
12	−190.03018	−190.02151	**11b**	−56.50589	−56.50208
12′	−190.04071	−190.03256	**13a**	−134.17666	−134.17161
TS(12′→14)	−189.97987	−189.97320	**16a**	−112.10149	−112.09719
14	−189.99207	−189.98520	**16b**	−77.83024	−77.82625
TS(14→15)	−189.92635	−189.91911	**17**	−56.13319	−56.12934
15	−189.99262	−189.98591			

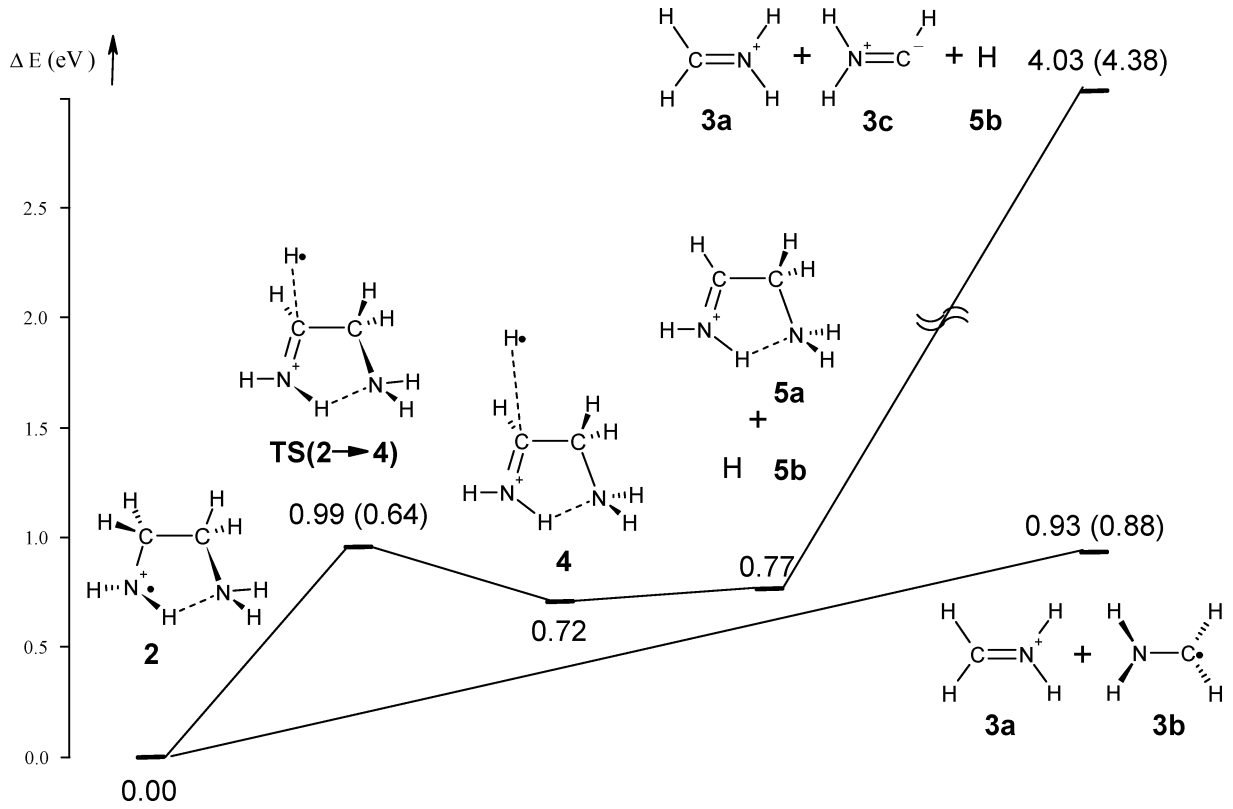

Figure 6. Gaussian-3 potential energy surface showing the possible mechanism for reaction 1a $NH_2CH_2CH_2NH_2^+ \rightarrow CH_2NH_2^+ + CH_2NH_2$, reaction 1b $NH_2CH_2CH_2NH_2^+ \rightarrow CH_2NH_2^+ + {}^-CHNH_2^+ + H$ and reaction 5 $NH_2CH_2CH_2NH_2^+ \rightarrow NH_2CH_2CHNH_2^+ + H$.

TABLE 3: Experimental and Calculated Energies (eV) of the Dissociations of En^+

dissociation reactions	ΔE(exp)	G3 reaction barrier
(1a) $NH_2CH_2CH_2NH_2^+ \rightarrow CH_2NH_2^+ + CH_2NH_2$	0.88 ± 0.04	0.93
(1b) $NH_2CH_2CH_2NH_2^+ \rightarrow CH_2NH_2^+ + {}^-CHNH_2^+ + H$	4.38 ± 0.04	4.03
(1c) $NH_2CH_2CH_2NH_2^+ \rightarrow CH_2NH_2^+ + CH_2 + NH_2$	7.17 ± 0.04	5.38
(2) $NH_2CH_2CH_2NH_2^+ \rightarrow CH_2{=}CHNH_2^+ + NH_3$	0.43 ± 0.03	0.62
(3) $NH_2CH_2CH_2NH_2^+ \rightarrow CH_2CH_2NH_2^+ + NH_2$	0.48 ± 0.03	0.62
(4) $NH_2CH_2CH_2NH_2^+ \rightarrow NH_3^+ + NH_2 + CH{=}CH_2$	6.12 ± 0.04	6.19
(5) $NH_2CH_2CH_2NH_2^+ \rightarrow NH_2CH_2CHNH_2^+ + H$	0.64 ± 0.04	0.99

cleavage of bond(s) or transition structure(s), are summarized in this section. Some major dissociation channels are described below.

(1) m/e = 30 (CH_4N^+). According to Figure 1, the $CH_2NH_2^+$ ion is the most abundant fragment ion at the VUV region. Cation $CH_2NH_2^+$ can be generated by breaking the C−C bond in en^+:

$$NH_2CH_2CH_2NH_2^+ \,(\mathbf{2}) + \Delta E_{1a} \rightarrow CH_2NH_2^+ \,(\mathbf{3a}) + CH_2NH_2 \,(\mathbf{3b})$$

$$\Delta E_{1a} = \mathrm{AE}(CH_2NH_2^+) - \mathrm{IE}(NH_2CH_2CH_2NH_2) = 0.88 \pm 0.04 \text{ eV} \quad (1a)$$

In the above mathematical expression, we have used our experimental IE and AE. The dissociation energies, along with those calculated by the G3 method (using the results listed in Table 2), are tabulated in Table 3 for easy comparisons. Here, ΔE_{1a} is the dissociation energy of this channel. The experimental ΔE of fragment $m/e = 30$ is 0.88 ± 0.04 eV. Our G3 results suggested that the product **3a** is formed by the homolytic C−C bond cleavage of parent ion **2**, involving no transition structure (TS). This pathway is pictorially shown in Figure 6 and the G3 dissociation energy is found to be 0.93 eV, in very good agreement with the experimental results. The energy cost for this straightforward reaction is not high, because the energy gained from the formation of a C−N π bond in **3a** partially compensates for the cleavage of the C−C bond. Therefore, this fragment is by far the most intense one among all fragment ions, and the dissociation channel is considered to be a dominant one.

There are two other onsets in the PIE spectrum at the higher energy region of 12.5−17.1 eV. We also calculated the dissociation energies of the following channels

$$NH_2CH_2CH_2NH_2^+ \,(\mathbf{2}) + \Delta E_{1b} \rightarrow CH_2NH_2^+ \,(\mathbf{3a}) + {}^-CHNH_2^+ \,(\mathbf{3c}) + H \,(\mathbf{5b})$$

$$\Delta E_{1b} = \mathrm{AE}(CH_2NH_2^+) - \mathrm{IE}(NH_2CH_2CH_2NH_2) = 4.38 \pm 0.06 \text{ eV} \quad (1b)$$

$$NH_2CH_2CH_2NH_2^+ \,(\mathbf{2}) + \Delta E_{1c} \rightarrow CH_2NH_2^+ \,(\mathbf{3a}) + CH_2 \,(\mathbf{3e}) + NH_2 \,(\mathbf{7b})$$

$$\Delta E_{1c} = \mathrm{AE}(CH_2NH_2^+) - \mathrm{IE}(NH_2CH_2CH_2NH_2) = 7.17 \pm 0.06 \text{ eV} \quad (1c)$$

For reaction 1b, computational results suggest a pathway in which a zwitterion **3c** is produced together with fragment ion **3a**. The energy profile of this reaction is also displayed in Figure 6. First, parent ion **2** undergoes a C−H bond fission via **TS-(2→4)** to yield an ion−neutral complex (INC) **4**. The energy barrier involved is 0.99 eV. The interaction between the hydrogen atom and the fragment ion **5a** is very weak; only 0.05 eV is required to separate them. The energy sum of free **5a** and hydrogen is 0.77 eV above parent ion **2**. Afterward, through a heterolytic C−C bond cleavage, ion **5a** further fragments into ion **3a**, the same product as reaction 1a, and 1-aminomethylene

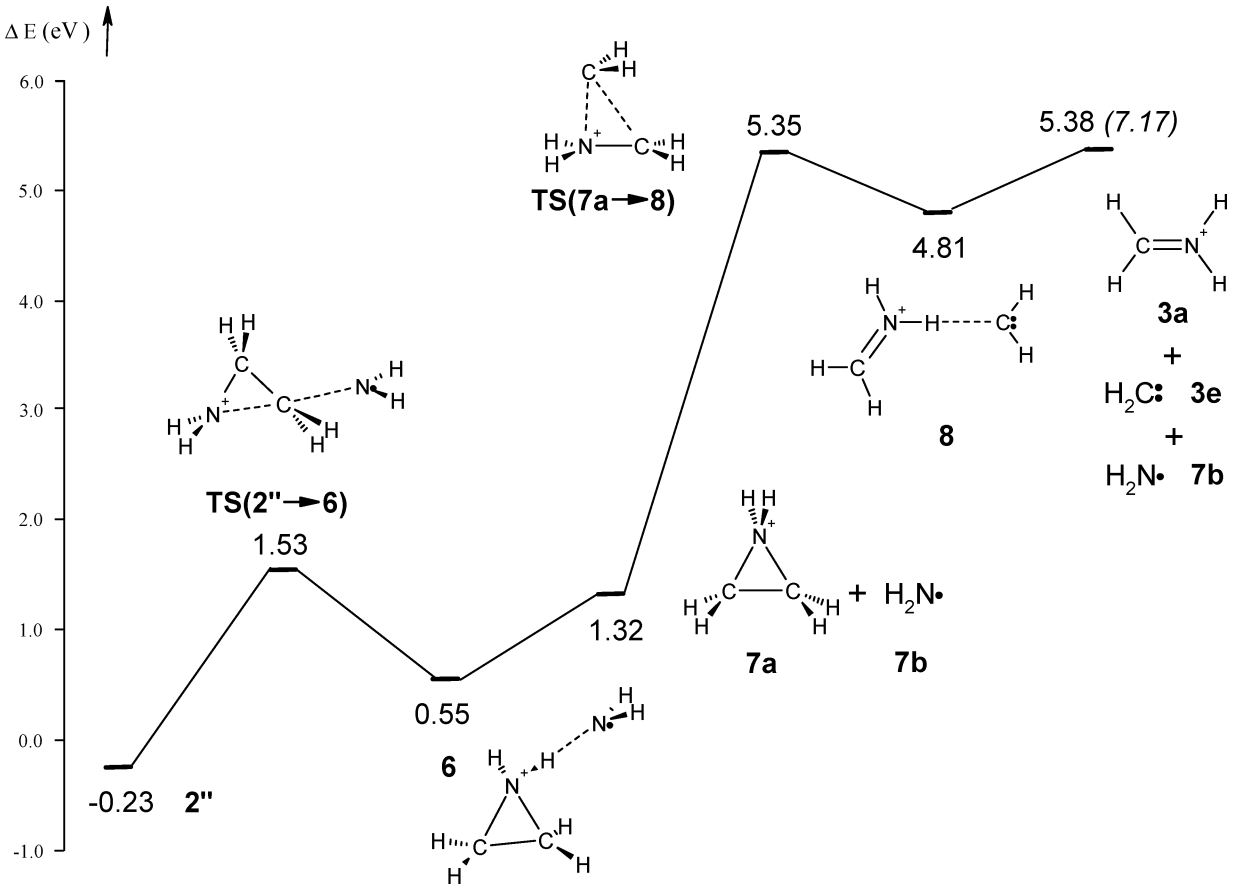

Figure 7. Gaussian-3 potential energy surface showing the possible mechanism for reaction 1c $NH_2CH_2CH_2NH_2^+ \rightarrow CH_2NH_2^+ + CH_2 + NH_2$.

(**3c**). Note that **3c** resembles a zwitterion more than a carbene. From the results of natural bond orbital (NBO) analysis,[20] it is seen that the C−N linkage is a double bond. The C═N double bond in **3c** (1.318 Å), being a bit longer than a "normal" C═N double bond (1.28 Å), reflects the instability of the geometry of **3c**. Calculations show that **3c** is far less stable than its isomer methanimine (CH_2NH), by about 1.7 eV. Hence, intuitively, methanimine may be proposed as a more plausible product instead of **3c** for this reaction. However, the formation of such a stable product unlikely involves a barrier as high as the observed value of 4.38 ± 0.06 eV. The G3 energy sum of **3a**, **3c** and hydrogen atom is 4.03 eV, which is in rough agreement with the experimental value.

The third onset observed at 15.59 ± 0.06 eV for ion with $m/e = 30$, as shown in Figure 3, requires yet another dissociation channel that also produces ion **3a**. The dissociation energy involved is much higher than the two pathways discussed above. The suggested mechanism for this reaction is presented in Figure 7. In this pathway, the anti conformer of en^+, **2″**, which can be formed by isomerization of **2** (breaking of an intramolecular hydrogen bond), undergoes a homolytic C^3-N^4 bond cleavage via **TS(2″→6)**. This TS is 1.53 eV above **2** and it involves a cyclization step forming a three-membered heterocyclic ring. Subsequently, energy is minimized by the migration of amino radical, NH_2, to facilitate hydrogen bonding, yielding complex **6**. The stabilization energy of this complex is about 0.77 eV. Dissociation of complex **6** produces free protonated aziridine (**7a**) and NH_2 radical (**7b**). Note that the G3 energy of NH_2 is included starting from this step, to enable comparison in energetics in the energy profile shown in Figure 7. Afterward, fragment ion **7a** undergoes a methylene elimination via **TS-(7a→8)**, which may be taken as the reverse of the electrocyclic reaction between singlet CH_2 carbene with methanimium ion. The elimination of CH_2 is asynchronous. As shown in Figure 5, the C^2-N^1 bond (2.199 Å) is shorter than the C^2-C^3 bond (2.512 Å) in **TS(7a→8)**. This step involves a substantial barrier, computed to be 4.03 eV. The INC **8** yielded then dissociates to produce **3a**, with an energy cost of 0.57 eV. The G3 energy sum of the fragment **3a**, methylene (**3e**) and **7b** is 5.38 eV. Because this step has the highest energy along the pathway, its energy is taken as the calculated dissociation energy. Unfortunately, this value is still much lower than the observed value of 7.17 eV. If the dissociation products are suggested to be **3a**, **3e**, nitrene (NH) and hydrogen, the energy sum is as high as 9.53 eV instead. We have not succeeded in establishing a pathway with calculated dissociation energy intermediate between these two extremes. In any event, the pathway shown in Figure 7 is the most probable mechanism we could propose.

(2) $m/e = 43$ ($C_2H_5N^+$). Cation $C_2H_5N^+$ may be generated through the elimination of NH_3 from the en^+:

$$NH_2CH_2CH_2NH_2^+ \textbf{(2)} + \Delta E_2 \rightarrow CH_2{=}CHNH_2^+ \textbf{(11a)} + NH_3 \textbf{(11b)}$$

$$\Delta E_2 = AE(CH_2{=}CHNH_2^+) - IE(NH_2CH_2CH_2NH_2) = 0.43 \pm 0.04 \text{ eV} \quad (2)$$

Fragment $m/e = 43$ contributes a fairly strong peak in the mass spectrum. The experimental dissociation energy of this ion is 0.43 ± 0.04 eV. The energy profile of this reaction is displayed in Figure 8. Similar to reaction 1c, this reaction

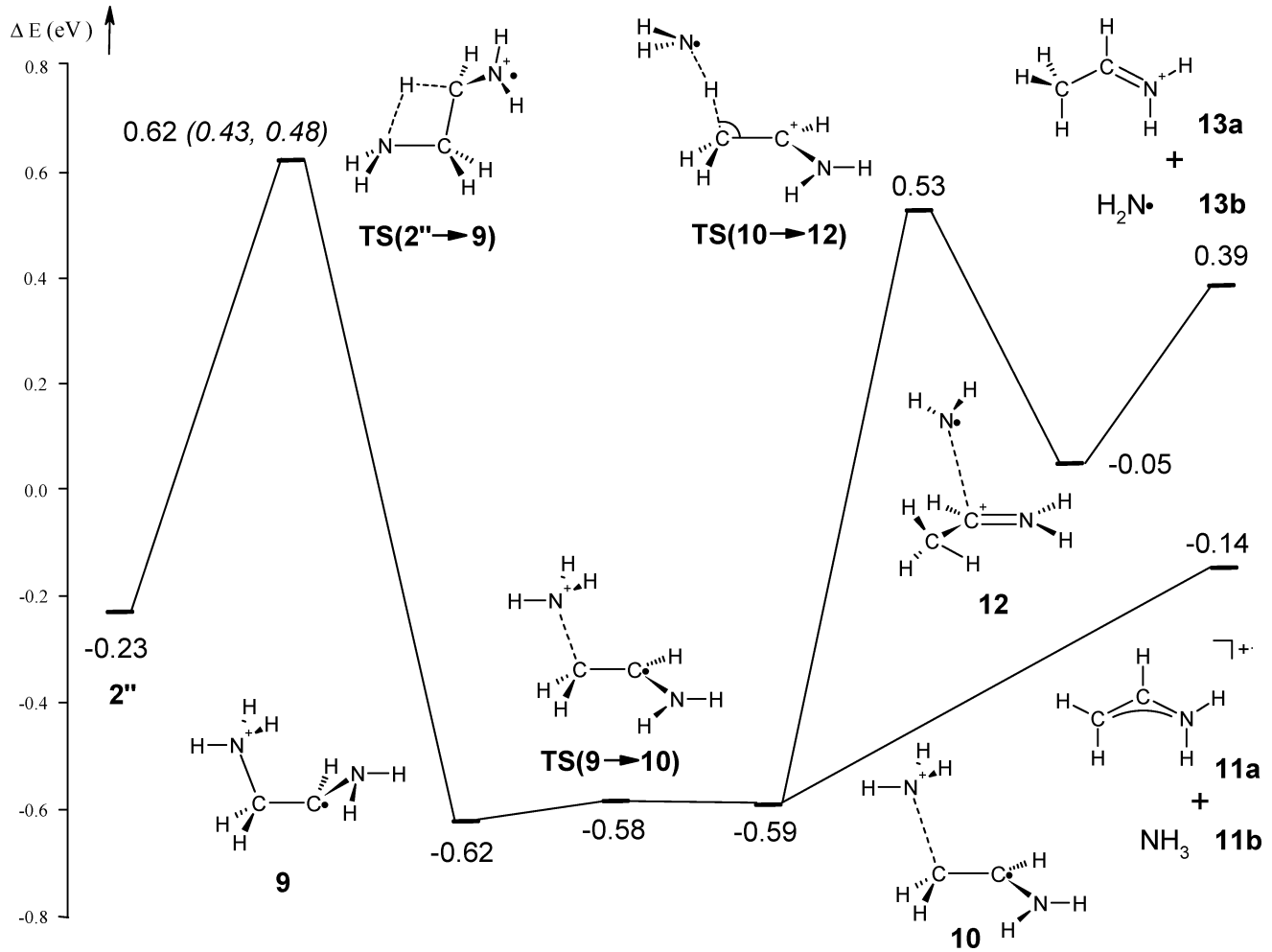

Figure 8. Gaussian-3 potential energy surface showing the possible mechanism for reaction 2 $NH_2CH_2CH_2NH_2^+ \rightarrow CH_2CHNH_2^+ + NH_3$ and reaction 3 $NH_2CH_2CH_2NH_2^+ \rightarrow CH_3CHNH_2^+ + NH_2$.

involves the isomerization of **2** to **2″**, with the latter more stable than the former by 0.23 eV. Upon a 1,3-hydrogen shift via **TS-(2″→9)**, distonic ion **9**, with a positive charge on N^1 and an unpaired electron on C^3, is produced. The energy barrier involved is 0.85 eV. From its structure shown in Figure 5 and the result of NBO analysis, it can be seen that hyperconjugation, i.e., the delocalization of the unpaired electron on C^3 into the $\sigma^*(N^1-C^2)$ orbital, significantly weakens the N^1-C^2 bond. Thus, a slightly longer N^1-C^2 bond length of 1.552 Å results. Yet the net effect is moderately stabilizing; distonic ion **9** is 0.62 eV below parent **2**. Elimination of NH_3 via **TS(9→10)** then takes place, producing INC **10**. The energy cost of this step is unexpectedly low, only 0.04 eV, which can be explained by the resonance effect. The partial positive charge on C^2 is readily dispersed to C^3 and N,[4] facilitated by the π overlap in this TS. As a result, the C^2-C^3 bond is markedly shortened. Finally, dissociation of INC **10** yields cation **11a** and ammonia (**11b**) as products, which involves a net barrier of 0.45 eV. The overall exothermicity of this reaction is 0.14 eV, which is primarily due to the stability **11a**; the delocalization of charge and unpaired electron in the π orbitals greatly lowers its energy. The overall barrier of reaction 2 is 0.62 eV, which is the energy of **TS(2″→9)** relative to **2**. It is fair accord with the experimental value of 0.43 ± 0.04 eV. It is noted that tunneling is important in some hydrogen migration processes.[21] If tunneling is involved here, there may be a lower energy barrier, which leads to better agreement with experiment.

(3) m/e = 44 ($C_2H_6N^+$). Cation $NH_2CH_2CH_2^+$ may be generated through the following reaction:

$$NH_2CH_2CH_2NH_2^+ + \Delta E_3 \rightarrow CH_3CH{=}NH_2^+ \textbf{(13a)} + NH_2 \textbf{(13b)}$$

$$\Delta E_3 = AE(CH_3CH{=}NH_2^+) - IE(NH_2CH_2CH_2NH_2) = 0.48 \pm 0.04 \text{ eV} \quad (3)$$

The experimental dissociation energy of fragment *m/e* = 44 is 0.48 ± 0.04 eV. This observed value is in large discrepancy with the G3 energy of **TS(2″→6)** relative to **2** (1.53 eV), as shown in Figure 7. Therefore, fragment *m/e* = 44, instead of being a side product branched from process (1c), requires an independent dissociation channel for its formation.

The proposed pathway for this reaction is also summarized in Figure 8. Basically, reaction 3 is a process branched from reaction 2, rather than a straightforward C−N bond dissociation of parent **2**. Instead of dissociating into **11a** and **11b**, INC **10** undergoes a hydrogen atom transfer via **TS(10→12)** to form another INC **12**. This process is better described as a hydrogen abstraction from ammonia by **11a**, involving a barrier of 1.12 eV. Subsequent dissociation of INC **12** produces cation **13a** and NH_2 (**13b**). The G3 energy sum of **13a** and **13b** is 0.39 eV above the parent **2**. Due to the formation of a resonance-stabilized species **13a**, the overall reaction is not highly

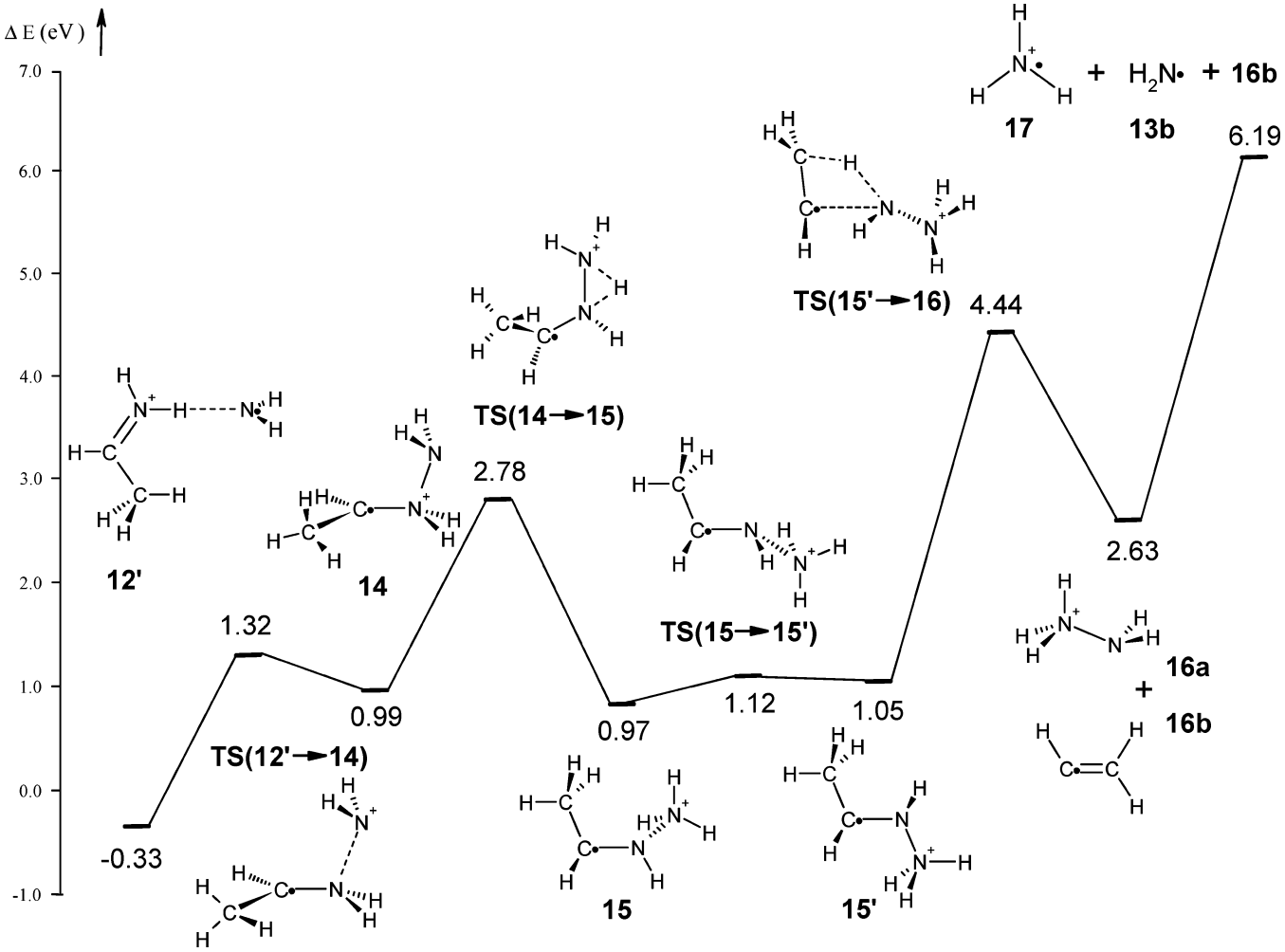

Figure 9. Gaussian-3 potential energy surface showing the possible mechanism for reaction 4 $NH_2CH_2CH_2NH_2^+ \rightarrow NH_3^+ + NH_2 + CH_2CH$.

endothermic. Again, **TS(2″→9)** is the highest energy step along the entire pathway starting from **2″**. Regarding the energy of **TS(2″→9)** (0.62 eV relative to **2**) as the calculated barrier, it is in fair agreement with the observed value of 0.48 ± 0.04 eV. As previously mentioned, tunneling may lead to a lower dissociation barrier for this step and as well as for **TS(10→12)**, because both of them involve hydrogen atom transfer. Nevertheless, the energy barrier is bounded by the energy sum of products pair of **13a** and **13b** (0.39 eV), which is in turn in better agreement with the experimental value.

(4) m/e = 17 (NH_3^+). Cation NH_3^+ may be generated through the following reaction:

$$NH_2CH_2CH_2NH_2^+ \textbf{(2)} + \Delta E_4 \rightarrow NH_3^+ \textbf{(17)} + NH_2 \textbf{(13b)} + CH_2{=}CH \textbf{(16b)}$$

$$\Delta E_4 = AE(NH_3^+) - IE(NH_2CH_2CH_2NH_2) = 6.12 \pm 0.04 \text{ eV} \quad (4)$$

The experimental ΔE of fragment $m/e = 17$ is 6.12 ± 0.04 eV. One may intuitively think that the fragment with $m/e = 17$ comes from water, as OH^+ also has the same mass-to-charge ratio. We have the proof to rule out the contribution from dissociative photoionization of water. The AE of OH^+ from water is 18.08 ± 0.05 eV,[22] and that of the IE of OH is 13.017 ± 0.002 eV, whereas the experimental AE of this fragment ($m/e = 17$) is 14.54 ± 0.04 eV. The current experimental value is lower than the AE of OH^+ from water, and higher than the IE of OH radical. This indicates that mass 17 is not OH^+. The formation of the ammonia cation inevitably requires a hydrogen shift. Moreover, the positive charge is on the nitrogen atom alone. Such an electronic structure is far less favorable than those of **3a**, **11a** and **13a**. Therefore, clearly a subtle dissociation mechanism is involved in the formation of $m/e = 17$.

Our G3 results suggest that this reaction is actually an extension of reaction 3. Instead of releasing free **13a** and **13b**, INC **12** first allows the NH_2 radical to migrate to another side to form a hydrogen bond with the electropositive hydrogen on N^1, resulting another INC **12′**. This alternative geometry is so stable that INC **12′** has its energy 0.33 eV below that of **2**. Afterward, as shown in Figure 9, the NH_2 radical attacks the $N^2{-}C^3$ π bond, via **TS(12′→14)** to form **14**, in which a new N−N single bond is formed. This radical addition entails an activation energy of 0.99 eV. Intermediate **14** is a distonic radical ion. However, unlike the situation in **9** (also distonic), it seems that the unpaired electron on C^3 does not weaken the $N^1{-}N^2$ bond appreciably, implying a low extent of hyperconjugation. Thus ion **14** is not exceptionally stable and has an energy of 0.99 eV relative to **2**. Subsequently, ion **14** undergoes a hydrogen shift from N^2 to N^1 via **TS(14→15)**, yielding another distonic radical ion **15**. Such a process involves a high energy barrier of 1.79 eV. According to NBO analysis, there is significant donation of electron density from the lone pair of N^2 into the half-filled 2p orbital of C^3. Yet ion **15** is barely more stable than **14** by 0.02 eV. Via a low-barrier C−N bond rotation (0.15 eV), **15** interconverts to another conformer **15′**,

which is slightly less stable than the former by less than 0.1 eV. Afterward, intermediate **15′** undergoes a syn-elimination of protonated hydrazine ion, $NH_2NH_3^+$ (**16a**). This process takes place through **TS(15′→16)** in which the N−C bond and C−H bond are asynchronously cleaved. The fission of N−C is essentially complete in **TS(15′→16)** because the N−C distance is stretched to a length of 2.242 Å. The resulting fragments, ion **16a** and vinyl radical (**16b**), do not form any collision complex after the syn-elimination. Eventually, homolytic N−N bond cleavage in **16a** without TS produces the ammonia cation (**17**) as the final product. The energy sum of all the dissociation products, namely **17**, **16b** and **13b**, is calculated to be 6.19 eV. It is in very good accord with the experimental dissociation energy of 6.12 ± 0.04 eV.

(5) m/e = 59 ($C_2H_7N_2^+$). Cation $C_2H_7N_2^+$ may be generated by the elimination of hydrogen atom from the en^+:

$$NH_2CH_2CH_2NH_2^+ \text{ (2)} + \Delta E_5 \rightarrow NH_2CH_2CHNH_2^+ \text{ (5a)} + H \text{ (5b)}$$

$$\Delta E_5 = AE(NH_2CH_2CHNH_2^+) - IE(NH_2CH_2CH_2NH_2) = 0.64 \pm 0.04 \text{ eV} \quad (5)$$

The dissociation energy measured here is rather low compared to the bond energies of C−H and N−H bonds. Because an N−H bond is known to be generally stronger than a C−H bond, we have simply ruled out the possibility of the formation of fragment ion *m/e* = 59 by N−H bond cleavage. Therefore, the proposed mechanism for this reaction simply consists of the first few steps of the dissociation channel for reaction 1b shown in Figure 6. The only TS involved is **TS(2→4)**, which is computed to be 0.99 eV above **2**. A facile dissociation of INC **4** releases free **5a** and a hydrogen atom. The sum of their energies is 0.77 eV relative to the parent ion. The newly formed N^1-C^2 π bond in **5a** partially subsidizes the loss of C−H bond energy, making the overall reaction less endothermic. The G3 barrier of 0.99 eV seems not be in good agreement with the observed value of 0.64 ± 0.04 eV. Nevertheless, as discussed above, tunneling of hydrogen probably results in a lower effective reaction barrier. If tunneling permits the C−H bond cleavage to proceed with an energy of 0.2 eV less than the activation energy, then the G3 reaction energy can still be said to be in satisfactory agreement with that of experimental value.

The PIE spectra for some other fragment ions, including CH_3^+, $C_2H_3^+$, $C_2H_4^+$, CH_4N^+, $C_2H_4N^+$, $C_2H_6N^+$, $C_2H_4N_2^+$, $C_2H_5N_2^+$, $C_2H_6N_2^+$, were measured also, but the signals are very weak. Thus the formation of these fragments is not considered in this initial study of ethylenediamine.

Conclusion

We have measured the IE of $NH_2CH_2CH_2NH_2$ and the AEs of fragment ions CH_4N^+, NH_3^+, $C_2H_5N^+$, $C_2H_6N^+$, and $C_2H_7N_2^+$ in the dissociative photoionizations of ethylenediamine with synchrotron radiation VUV photoionization mass spectrometry. With the aid of ab initio Gaussian-3 results, we have analyzed the dissociation channels for the formation of these fragment ions. The energies of some proposed channels are in rough to very good agreement with experiment, whereas some are not in agreement at all. These dissociation channels have been described and discussed in some detail.

Acknowledgment. F.Q. is thankful for the funding support from Natural Science Foundation of China under Grant No 20473081 and 20533040, Chinese Academy of Sciences (CAS), SRF for ROCS of SEM, and SRFDP.

References and Notes

(1) Kimura, K.; Katsumata, S.; Achiba, Y.; Yamazaki, T.; Iwata, S. *Ionization energies, Ab initio assignments and valence electronic structure for 200 molecules: Handbook of HeI Photoelectron Spectra of Fundamental Organic Compounds*; Japan Scientific Society Press: Tokyo, 1981.

(2) Burkey, T. J.; Castelhano, A. L.; Griller, D.; Lossing, F. P. *J. Am. Chem. Soc.* **1983**, *105*, 4701.

(3) Radom, L.; Lathan, W. A.; Hehre, W. J.; Pople, J. A. *J. Am. Chem. Soc.* **1973**, *95*, 693.

(4) Alsenoy, C. V.; Siam, K.; Ewbank, J. D.; Schäfer, L. *J. Mol. Struct.: THEOCHEM* **1986**, *136*, 77.

(5) Kazerouni, M. R.; Hedberg, L.; Hedberg, K. *J. Am. Chem. Soc.* **1994**, *116*, 5279.

(6) Lee, S. J.; Mhin, B. J.; Cho, S. J.; Lee, J. Y.; Kim, K. S. *J. Phys. Chem.* **1994**, *98*, 1129.

(7) Chang, Y.-P.; Su, T.-M.; Li, T.-W.; Chao, I. *J. Phys. Chem. A* **1997**, *101*, 6107.

(8) Kudoh, S.; Takayanagi, M.; Nakata, M.; Ishibashi, T.; Tasumi, M. *J. Mol. Struct.* **1999**, *479*, 41.

(9) Carvalho, L. A. E. B. d.; Lourenço, L. E.; Marques, M. P. M. *J. Mol. Struct.* **1999**, *482−483*, 639.

(10) Tsierkezos, N. G.; Schroder, D.; Schwarz, H. *Int. J. Mass Spectrom.* **2004**, *235*, 33.

(11) Wang, X.; Yang, D.-S. *J. Phys. Chem. A* **2004**, *108*, 6449.

(12) Li, S.; Fuller, J. F.; Wang, X.; Sohnlein, B. R.; Bhowmik, P.; Yang, D.-S. *J. Chem. Phys.* **2004**, *121*, 7692.

(13) Liu, F.; Qi, F.; Gao, H.; Sheng, L.; Zhang, Y.; Yu, S.; Lau, K.-C.; Li, W.-K. *J. Phys. Chem. A* **1999**, *103*, 4155.

(14) Wei, L.; Yang, B.; Yang, R.; Huang, C.; Wang, J.; Shan, X.; Sheng, L.; Zhang, Y.; Qi, F.; Lam, C.-S.; Li, W.-K. *J. Phys. Chem. A* **2005**, *109*, 4231.

(15) Qi, F.; Sheng, L.; Zhang, Y.; Yu, S.; Li, W.-K. *Chem. Phys. Lett.* **1995**, *234*, 450.

(16) Sheng, L.; Qi, F.; Tao, L.; Zhang, Y.; Yu, S.; Wong, C.-K.; Li, W.-K. *Int. J. Mass Spectrom. Ion Processes* **1995**, *148*, 179.

(17) Sheng, L.; Qi, F.; Gao, H.; Zhang, Y.; Yu, S.; Li, W.-K. *Int. J. Mass Spectrom. Ion Processes* **1997**, *161*, 151.

(18) Huang, C. Q.; Yang, B.; Yang, R.; Wang, J.; Wei, L. X.; Shan, X. B.; Sheng, L. S.; Zhang, Y. W.; Qi, F. *Rev. Sci. Instrum.* **2005**, *76*, 126108.

(19) Frisch, M. J.; Trucks, G. W.; Schlegel, H. B.; Scuseria, G. E.; M. A. Robb; Cheeseman, J. R.; Montgomery, J. A., Jr.; Vreven, T.; Kudin, K. N.; Burant, J. C.; Millam, J. M.; Iyengar, S. S.; Tomasi, J.; Barone, V.; Mennucci, B.; Cossi, M.; Scalmani, G.; Rega, N.; Petersson, G. A.; Nakatsuji, H.; Hada, M.; Ehara, M.; Toyota, K.; Fukuda, R.; Hasegawa, J.; Ishida, M.; Nakajima, T.; Honda, Y.; Kitao, O.; Nakai, H.; Klene, M.; Li, X.; Knox, J. E.; Hratchian, H. P.; Cross, J. B.; Bakken, V.; Adamo, C.; Jaramillo, J.; Gomperts, R.; Stratmann, R. E.; Yazyev, O.; Austin, A. J.; Cammi, R.; Pomelli, C.; Ochterski, J. W.; Ayala, P. Y.; Morokuma, K.; Vot, G. A.; Salvador, P.; Dannenberg, J. J.; Zakrzewski, V. G.; Dapprich, S.; Daniels, A. D.; Strain, M. C.; Farkas, O.; Malick, D. K.; Rabuck, A. D.; Raghavachari, K.; Foresman, J. B.; Ortiz, J. V.; Cui, Q.; Baboul, A. G.; Clifford, S.; Cioslowski, J.; Stefanov, B. B.; Liu, G.; Liashenko, A.; Piskorz, P.; Komaromi, I.; Martin, R. L.; Fox, D. J.; Keith, T.; Al-Laham, M. A.; Peng, C. Y.; Nanayakkara, A.; Challacombe, M.; Gill, P. M. W.; Johnson, B.; Chen, W.; Wong, M. W.; Gonzalez, C.; Pople, J. A. *Gaussian 03*, revision B.05 ed.; Gaussian, Inc: Wallingford, CT, 2004.

(20) Reed, A. E.; Curtiss, L. A.; Weinhold, F. *Chem. Rev.* **1988**, *88*, 899.

(21) Bell, R. P. *The Tunnel Effect in Chemistry;* Chapman and Hall Ltd.: London and New York, 1980.

(22) Lefaivre, D.; Marmet, P. *Can. J. Phys.* **1978**, *56*, 1549.